Nanoscale

Accepted Manuscript

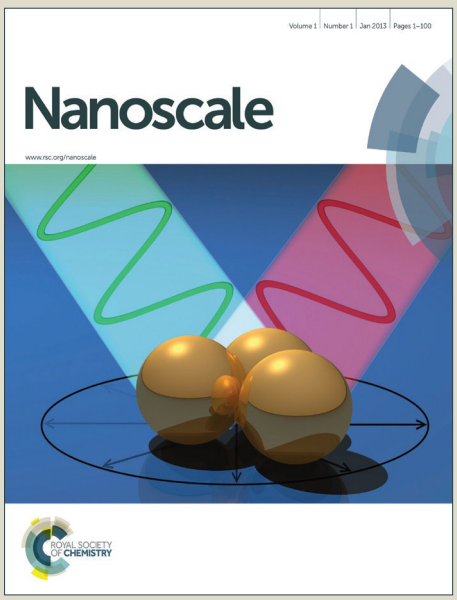

ROYAL SOCIETY OF CHEMISTRY

www.rsc.org/nanoscale

Nanoscale

ARTICLE

Tuning photoluminescence and surface properties of carbon nanodots for chemical sensing

Received 00th January 20xx,
Accepted 00th January 20xx

DOI: 10.1039/x0xx00000x

www.rsc.org/

*Zhaomin Zhang,[a] Yi Pan,[a] Yaning Fang,[a] Lulu Zhang,[a] Junying Chen,[a] Changqing Yi[a]**

Obtaining tunable photoluminescence (PL) with improved emission properties is crucial for successfully implementing fluorescent carbon nanodots (fCDs) in all practical applications such as multicolour imaging and multiplexed detection by a single excitation wavelength. In this study, we report a facile hydrothermal approach to adjust PL peaks of fCDs from blue, green to orange by controlling the surface passivation reaction during the synthesis. This is achieved by tuning the passivating reagents in a step-by-step manner. The as-prepared fCDs with narrow size distribution show improved PL properties with different emission wavelength. Detailed characterization of fCDs using elemental analysis, Fourier transform infrared spectroscopy, and X-ray photoelectron spectroscopy suggested that the surface chemical composition results in this tunable PL emission. Surface passivation significantly alters the surface status, resulting in fCDs with either stronger surface oxidation and N element doping that ultimately determine their PL properties. Further experiments suggested that the as-prepared orange luminescent fCDs (O-fCDs) were the sensitive and specific nanosensing platforms towards Fe^{3+} determination in complex biological environment, emphasizing its potential practical applications in clinical and biological fields.

1. Introduction

Fluorescent carbon nanodots (fCDs) which comprise a graphene-based core and carbonaceous surface, promote the development of high performance nanosensors, novel biomedical imaging probes, and multifunctional nano-composites for theranostics, because of their superior optical and nontoxic features[1-10]. Various approaches, such as laser ablation, electrochemical etching, microwave and ultrasonic shearing, plasma-etching and pyrolysis, have been demonstrated to prepare fCDs with different emission wavelength[4-10]. Those attempts have significance for the development and applications of fCDs, but exploring approaches to synthesize fCDs with tunable emission is still a great challenge, due to the lack of sufficient theoretical and experimental knowledge on fCDs. The difficulty in preparing long-wavelength emissive fCDs constitutes another major disadvantage of current synthesis strategies.

Obtaining tunable photoluminescence (PL) and improved quantum yields is crucial for successfully implementing fCDs in all practical applications such as multicolour imaging and multiplexed detection by a single excitation wavelength[11-33]. It has been reported that most fCDs exhibit excitation-dependent PL characteristics where the emission-peaks shift towards longer wavelength with much weaker intensity than their dominant emission when varying the excitation wavelength bathochromically[27-33]. However, that does not constitute true tuning and is usually undesired in practical applications[19]. Therefore, tremendous effort has been spent on developing rational strategies to investigate intrinsic PL properties of fCDs and thus tuning their emission[11-34]. It has been reported that fCDs with luminescence emission across the entire visible spectrum can be finely tuned by controlling the dehydrating agents, the reaction temperature and time to control the nucleation and growth kinetics[16,19,20,22,26]. Through simply adjusting the molar ration of the reactants, the tunable emission of fCDs can be achieved using one-pot pyrolysis approaches[11,15,17]. Doping fCDs with heteroatom such as N, S, or Se, is another important route to tune their PL properties[12-14]. By varying the applied potentials and carbonization temperature using top-down strategies, fCD size can be tuned, and thus their PL properties[18,24,25]. Despite this, continued efforts should be exerted to explore efficient strategies for synthesizing fCDs with tunable emission, especially with long-wavelength emission which favors the *in vitro* and *in vivo* bioimaging, since it is still elusive thus far.

Herein, we report a facile hydrothermal approach to adjust PL peaks of fCDs from blue, green to orange by controlling the surface passivation reaction during the synthesis. This is achieved by tuning the passivating reagents in a step-by-step manner. Our synthetic route is illustrated in Figure 1. Firstly, fCDs with blue emission (B-fCDs) were prepared by a one-step hydrothermal route using non-conjugated polymers PEG_{400} (polyethylene glycol (PEG) with a molecular weight of 400

[a] *Key Laboratory of Sensing Technology and Biomedical Instruments (Guangdong Province), School of Engineering, Sun Yat-Sen University, Guangzhou, China. Email: yichq@mail.sysu.edu.cn; Tel: 86-20-39342380.*

†Electronic Supplementary Information (ESI) available: [details of any supplementary information available should be included here]. See DOI: 10.1039/x0xx00000x

g mol^{-1}) as the sole carbon source[35]. Then, PEG_{1000} (PEG with a molecular weight of 1000 g mol^{-1}) was added into the reaction system for surface passivating the resultant B-fCDs to synthesize fCDs with green emission (G-fCDs). At last, further surface passivation of the resultant G-fCDs with 2,2'-(Ethylene-dioxy)-bis(ethylamine) (EDA, $H_2NCH_2CH_2OCH_2CH_2OCH_2CH_2NH_2$) enabled the preparation of fCDs with orange emission (O-fCDs). This new bottom-up synthetic strategy leads to highly stable crystalline fCDs with tunable PL and surface properties in high reproducibility. Moreover, the potential of the orange luminescent fCDs as nanosensing platform towards sensitive Fe^{3+} detection was explored.

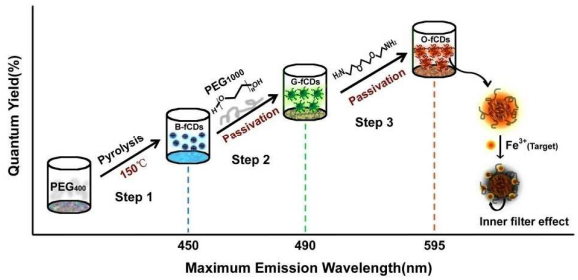

Figure 1. Schematic illustration of the synthetic routes for fCDs with different emission colors and the mechanism of O-fCDs as specific nanoprobes towards Fe^{3+} detection.

2. Experimental

2.1 Apparatus

The morphology and size distribution of the fCDs were characterized with a transmission electron microscope (TEM, JEOL JEM-1400) and a NanoZS90 instrument (Malvern), respectively. UV-Vis, fluorescence and ^{1}H NMR spectra were scanned using a DU730 UV-Vis spectrometer (Beckman), a Fluoromax-4P spectrometer (Horiba) and an INOVA500NB NMR spectrometer (Varian), respectively. Fluorescence lifetime and the absolute quantum yield of fCDs were measured on a Fluorolog-3 spectrometer equipped with Quanta-ϕ accessory and Photoluminescence Quantum Yields (PLQY) software package (Horiba). Characterization of fCD surface properties were conducted on a VERTEX 70 spectrometer (Bruker) and an ESCALab250 spectroscopy (Thermo Fisher), respectively. Elemental analysis results were obtained on a VarioEL elemental analyzer (Elementar).

2.2 Synthesis of fCDs with different emission colors

B-fCDs were synthesized by low temperature pyrolysis of PEG_{400} (Sinopharm Chemical Reagent Co., Ltd), according to a previous report by Fan and co-workers[35]. Briefly, 15 mL PEG_{400} was added into a round-bottom flask and heated at 150℃ for 12 hours until a faint yellow solution was formed. The solution was subsequently subjected to dialysis for 3 days to collect B-fCDs. For the preparation of G-fCDs, 2 g PEG_{1000} was added into the above faint yellow solution and allowed to react for another 6h at 150℃, until a gold yellow solution was formed. Subsequently, the solution was subjected to dialysis for 3 days to collect G-fCDs. In order to obtain highly luminescent O-fCDs, 200 μL EDA was added into the above gold yellow solution and allowed to react for another 1.0-1.5 h at 150℃, until a brown solution was formed. D.I water was gradually added into the brown solution and centrifuged at 10,000 rpm for 15 min. Then, the supernatant was subjected to dialysis for 3 days to collect O-fCDs. The as-prepared fCDs were purified by silica gel column chromatography, as described in detail elsewhere[29,36]. Finally, the purified fCDs were lyophilized and stored at 4℃ before further usage.

2.3 Metal ion detection

The metal ion solutions were prepared from $FeCl_3$, $NiCl_2$, $AgNO_3$, $CoCl_2$, $ZnCl_2$, $CrCl_3$, $CdCl_2$, $AlCl_3$, $Pb(NO_3)_2$, $HgCl_2$, $GdCl_3$, $Cu(AC)_2$, $Mn(SO_4)_2$ in distilled water with a concentration of 50 μM. For metal ion detection, the calculated amount of Fe^{3+} (0, 1, 3, 5, 15, 20, 50, 100, 500, 1000 μM) was added to 1 mL Tris-HCl buffer solution (10 mM, pH=7.4) containing 500 μg O-fCDs, and allowed to react for 1 min under gentle shaking. Then, photographs were taken and fluorescence spectra were recorded. The interference assays were carried out by mixing 50.0 μM metal ions with O-fCDs (500 μg·mL^{-1}) under the optimized experimental conditions as the Fe^{3+} detection. All experiments were performed at room temperature.

3. Results and discussions

3.1 Synthesis of fCDs with different emission colors

Due to its non-toxic and non-immunogenic features, PEG has been extensively used as passivating agent or solvent to fabricate biocompatible fCDs[35,37-39]. Our synthetic route for fCDs with different emission colors starts from the B-fCDs which is prepared by a one-step hydrothermal route using PEG_{400} as the sole carbon source[35]. After hydrothermal reaction, the colorless and non-emissive PEG solution changed to faint yellow, where the resultant B-fCDs were well dispersed in water with transparent appearance and emitted blue PL under UV irradiation (Figure 2A).

Although the exact mechanism is still an open question, fCD's light emission can be attributed to quantum-size effect, emissive traps, structural defects induced by finite size and element doping, electron-hole recombination, and bandgap transitions corresponding to conjugated π-domains[5-10]. It has been demonstrated that fCDs having the appropriate surface functionalization could become semiconductor-like to exhibit bandgap-like electronic transition[39,40]. Therefore, it is possible to tune the quantum yield, life time, and the color of fCDs by passivating their surface. Enlightened by Sun's work, the surface passivation of B-fCDs using PEG_{1000} was carried out. As anticipated, after the surface passivation of B-fCDs using PEG_{1000}, not only the emission color was tuned to green (Figure

2A), but also the life time was significantly increased from 1.54 ns to 4.76 ns (Figure S1 & Table 1).

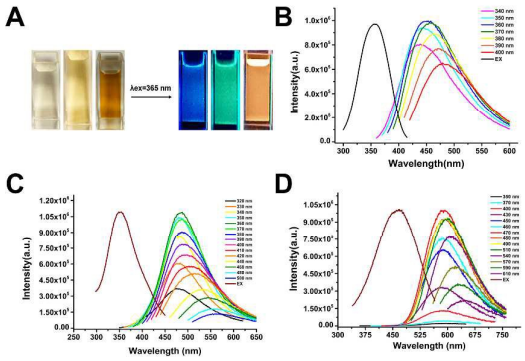

Figure 2. (A) Photographic images of B-fCDs, G-fCDs and O-fCDs dispersed in water in daylight (left), and under λ = 365 nm UV irradiation (right). (B-D) Excitation and wavelength-dependent PL emission spectra of (B) B-fCDs, (C) G-fCDs and (D) O-fCDs.

It is believed that C-N bonds can alter electronic structures of fCDs and/or generate additional low-energy band-gaps in fCDs, thus tuning their emission[13,14,16,26-28,39-42]. And it has been reported recently that the energy gap in the fCDs relies on the relative amount of different types of carbon bonding with N and O[19]. Therefore, in order to regulate the emission of fCDs towards longer wavelength, EDA was chosen for further surface passivating G-fCDs[42]. After the surface passivation reaction, the golden yellow solution of G-fCDs changed to a brown solution which contains highly dispersible O-fCDs (Figure 2A). Again, as expected, the emission color of fCDs was tuned to orange (Figure 2A), and the life time was further increased to 7.74 ns (Figure S1 & Table 1).

Table 1. Quantum Yield and Lifetime of B-fCDs, G-fCDs and O-fCDs.

Sample	Quantum Yield (%)	Life time (ns)
B-fCDs	4.61	1.54
G-fCDs	4.85	4.76
O-fCDs	5.32	7.74

As designed, the prepared fCDs exhibited different emission colors (blue, green and orange) under single-wavelength UV irradiation (Figure 2A). The strongest emission peaks of B-fCDs, G-fCDs and O-fCDs which reflect their dominant energy gap are around 450, 490, and 590 nm at the max excitation wavelength of 360, 360, 470 nm, respectively (Figure 2B, 2C & 2D). All fCDs exhibited a characteristic wavelength-dependent emission, for example, the emission peak of O-fCDs shifted from 590 to 640 nm under 400-610 nm excitation (Figure 2D), which may be attributed to a quantum confinement of emissive energy traps to the particle surface[36-40]. The exact fluorescence lifetimes for B-fCDs, G-fCDs and O-fCDs are listed in Table 1. Fluorescence lifetime of fCDs was significantly increased from 1.54 to 7.74 ns, possibly due to the suppression of non-radiative energy transitions induced by surface passivation[12]. All the prepared fCDs have fluorescence lifetime within the timescale of ns, indicating the singlet state nature of their emission[19]. Not only the fluorescence lifetime, but also the quantum yield (QY) of fCDs was obviously increased through step-by-step surface passivation, where the QY of B-fCDs, G-fCDs and O-fCDs was 4.61%, 4.85% and 5.31%, respectively. It is believed that the transformation of the pyrrolic N into graphite N under the hydrothermal condition can significantly improve the QY of fCDs[44]. All these results validate the significantly improved PL properties of fCDs through surface passivation.

3. 2 Characterization of fCDs with different emission colors

According to TEM observation, all the prepared fCDs are uniform in size, spherical in shape, and well dispersed in water (Figure 3A-3C). Dynamic light scattering (DLS) measurements reveal that B-fCDs G-fCDs and O-fCDs exhibit narrow size distribution in the range of 0.8-2.2, 2.0-7.0, and 4.0-10.0 nm, and have an average diameter of 1.5, 4.5 and 6.5 nm, respectively (Insets of Figure 3A-3C). As shown in the high-resolution TEM images, all the prepared fCDs, including B-fCDs, G-fCDs and O-fCDs, have lattice spacing of 0.20-0.22 nm which is consistent with that of (100) diffraction planes of graphite (Figure 3D, 3E & 3F), suggesting the surface passivation did not change the core crystalline structure of fCDs. These results are well correlated with the selected-area electron diffraction (SAED) patterns of B-fCDs, G-fCDs and O-fCDs (Figure S2).

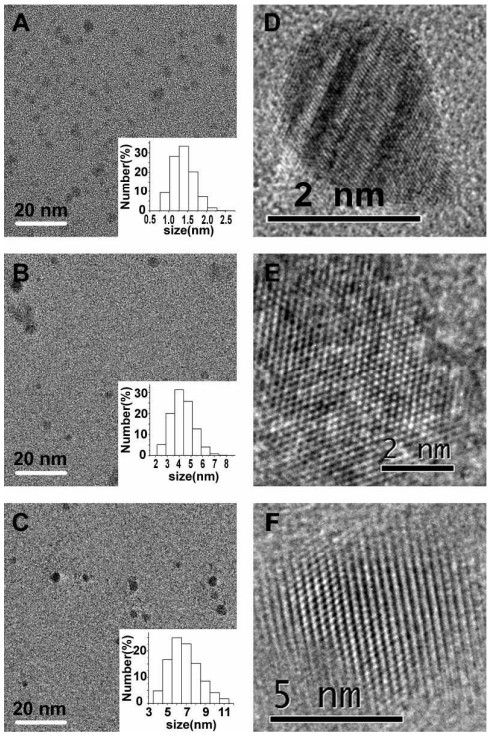

Figure 3. (A-C) TEM images of B-fCDs (A), G-fCDs (B) and O-fCDs (C). (D-E)HRTEM images of single nanoparticle with the lattice spacing of B-fCDs (D), G-fCDs (E) and O-fCDs (F). Inset shows the size distribution of fCDs.

Engineering the surface compositions of fCDs plays key roles not only in regulating their emission through tailoring their surface-related defective sites, but also in connecting fCDs with fascinating applications[1]. The surface chemical compositions of fCDs were characterized by elemental analysis, FTIR and XPS. The elemental analysis shows that all fCDs contain C, H, and O elements, while additional N element is presented in O-fCDs (Table S1). It is obvious from the elemental analysis results that all fCDs consist predominantly of C and O elements. In our synthetic route, more O element is expected to be incorporated into fCD's surface after the first step surface passivating B-fCDs with PEG_{1000} to produce G-fCDs. In the second step surface passivation using EDA as the passivation reagent, N element is expected to be doped into the resultant O-fCD's surface, thus changing the relative amount of carbon bonding with N and O. The composition variation correlated well with our synthetic route (Table S1).

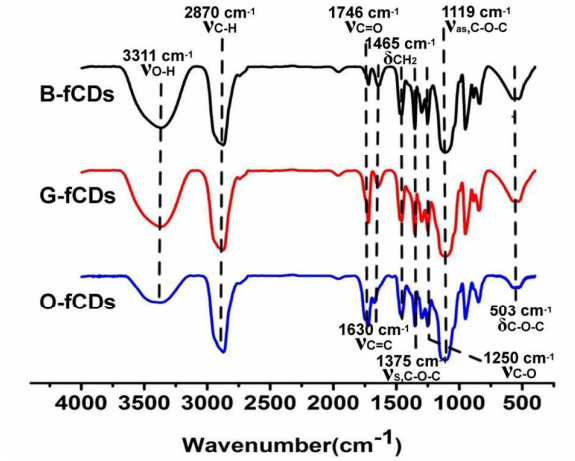

Figure 4. FTIR spectra of B-fCDs, G-fCDs and O-fCDs.

To further investigate the surface composition and their chemical state, fCDs were characterized by FTIR. FTIR spectra of B-fCDs, G-fCDs and O-fCDs were presented in Figure 4, revealing the existence of sufficient hydrophilic oxygen-containing functional groups. The broad band at *ca*. 3311 cm^{-1} is ascribed to the stretching vibration of -OH, whereas the bands at *ca*. 1375, 1119, and 503 cm^{-1} correspond to the asymmetric and symmetric stretching vibration, and bending vibration of C-O-C, respectively. The band at *ca*. 1746 cm^{-1} is ascribed to the stretching vibration of C=O. These oxygen-containing functional groups on fCDs surface were originated from the PEG which was cracked into small fragments containing the glycol structure during the hydrothermal synthesis[35], since the dehydration and carbonization are the major formation paths of fCDs[5-10]. Compared to B-fCDs, the absorption peak of $\nu_{C=O}$ at *ca*. 1746 cm^{-1} with significantly enhanced intensity and the absorption peak of ν_{O-H} at *ca*. 3311 cm^{-1} with obviously weakened intensity, was observed in the FTIR spectra of G-fCDs and O-fCDs. This result is quite important and provide strong evidence for successful surface oxidation of B-fCDs, since the hydrothermal process can generate lots of peroxyl radicals (HOO•) which can oxidize surface hydroxyl groups into carbonyl groups[35,43]. It has been reported previously that a higher degree of surface oxidation leads to the red-shifted PL emission, because surface defects brought by surface oxidation could introduce emission sites onto fCDs, thus varying the PL emission[24].

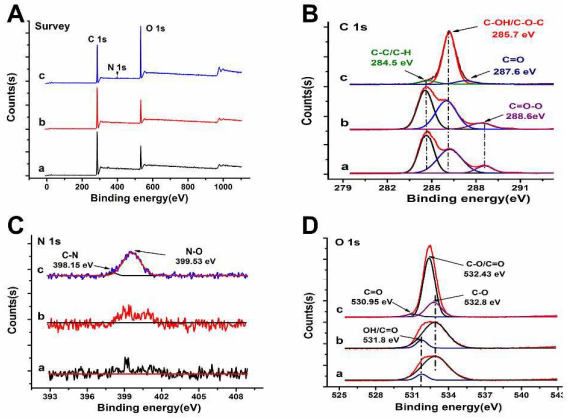

Figure 5. (A) XPS survey spectra of a) B-fCDs, b) G-fCDs, c) O-fCDs. (B) C 1s spectra of a) B-fCDs, b) G-fCDs, c) O-fCDs. (C) N 1s spectra of a) B-fCDs, b) G-fCDs, c) O-fCDs. (D) O 1s spectra of a) B-fCDs, b) G-fCDs, c) O-fCDs.

XPS surveys spectra confirm that B-fCDs and G-fCDs have the same elemental composition, showing the characteristic peaks corresponding to C 1s (286.2eV) and O 1s (532.4 eV). While, as expected, O-fCDs showed an additional characteristic peak corresponding to N 1s (399.5 eV), confirming the successful doping of N element after the second step surface passivation using EDA (Figure 5A). The deconvoluted XPS C 1s spectra presenting a peak at the binding energy of ~284.5 eV indicates the presence of graphitic sp^2 carbon structure in all fCDs (Figure 5B)[17,28], which agree well with SAED pattern results. The dominant peak centered at binding energies of 285.7 eV and the shoulder peak centered at binding energies of 288.6 eV are attributed to C-O and C=O groups, respectively (Figure 5B). It is obvious from the change of the C=O group intensity in Figure 5B that the surface oxidation degree was continuously deepened along with the step-by-step surface passivation reactions. These results confirm the presence of sufficient hydrophilic oxygen-containing functional groups on fCD's surface, correlating well with the FTIR result (Figure 4). And the diversity of oxygen containing functional groups possibly result in different emitting species in fCDs[12,19]. The high-resolution XPS N 1s spectra of O-fCDs exhibited a peak at 399.5 eV corresponding to N-O, while no such peak could be detected for B-fCDs and G-fCDs (Figure 5C). One peak centered at binding energies of ~532 eV which is attributed to C-O groups, is presented in the deconvoluted O 1s XPS spectra (Figure 5D).

Through carefully analysis of the above elemental analysis, FTIR and XPS data, the possible mechanism for tuning PL emission through step-by-step surface passivation is proposed. During hydrothermal synthesis, the PEG is cracked into small fragments containing the glycol structure for forming B-fCDs through dehydration and carbonization. In the first step surface passivation of B-fCDs using PEG_{1000}, the surface of B-fCDs is oxidized possibly by peroxyl radicals (HOO•) which are generated by the hydrothermal process[35,43]. Since surface oxidation can bring more surface defects and introduce more emission sites onto fCDs[24], the PL emission of B-fCDs can be tuned to longer wavelength to form G-fCDs. The FTIR results that the significantly enhanced absorption peak of $\nu_{C=O}$ and the obviously weakened absorption peak of ν_{O-H}, strongly support the oxidization of surface hydroxyl groups into carbonyl groups (Figure 4A). And the elemental analysis results that the oxygen-to-carbon ratio of fCDs is increased from 0.777 to 0.781 after the surface passivation also support our hypothesis. Then, in the second step surface passivation of G-fCDs using EDA, the surface of G-fCDs is doped with N elements. Since doping N elements can alter electronic structures of fCDs and/or generate additional low-energy band-gaps in fCDs[13,14,16,26-28,39-42], the PL emission of G-fCDs can be tuned to longer wavelength to form O-fCDs. The presence of a peak corresponding to C-N at XPS spectra and the elemental analysis result, provide the strong evidences for successful N-doping in O-fCDs. Actually, the N-doping might be a determinant factor for the synthesis of long-wavelength emissive fCDs, since no fCDs with emission wavelength longer than 570 nm can be synthesized without heteroatom (N, S, P, Se and etc.) doping thus far. Therefore, surface passivation significantly alters the surface status, resulting in fCDs with either stronger surface oxidation or N element doping that ultimately determine their photoluminescence properties. These relationships are believed, at least partially, to be responsible for this tunable PL emission of fCDs, and may help the community to control their PL properties. Definitely, more in depth studies are still required for further elucidation.

3. 3 Detection of Fe^{3+}

The oxygen functional groups on the surface of fCDs can not only facilitate their high water solubility, but also provide a possibility as a nanosensing platform for the metal ion detection due to the strong coordination between the oxygen functional groups and metal ions[11,12,45-48]. Considering that long-wavelength PL and excitation are critical needed in biomedical detection and bioimaging, we explored the feasibility of the O-fCDs as an optical nanoprobe for the detection of metal ions in aqueous solutions. As shown in Figure 6A, when 50.0 μM Fe^{3+} ions were introduced into the solution containing 500 μg·mL^{-1} of O-fCDs, the dramatic PL quenching was observed within 5 seconds, suggesting the rapid response of the present nanosensing system towards Fe^{3+}. The PL intensity of O-fCDs at 595 nm decreases linearly along with the increase of the Fe^{3+} concentration from 0.5 to 30.0 μM, while the quantification of Fe^{3+} could be achieved with a correlation coefficient of 0.998, indicating the excellent sensing properties towards trace Fe^{3+} detection (Figure 6B & 6C). The fluorescence quenching data follow Stern-Volmer equation: $F_0/F = 1 + K[Q]$ (Figure 6C), where [Q] is the concentration of Fe^{3+}, and F_0 and F are PL intensities of O-fCDs at 595 nm in the absence and presence of Fe^{3+}, respectively. The lowest detection limit (LOD) is calculated to be 0.43 μM based on the standard deviation of the response (SD) and the slope of the calibration curve (S) at levels approximating the LOD according to the formula: LOD = 3.0 (SD/S). It has been reported that the concentration of Fe^{3+} in serum is in the range of 7.52 - 11.8 mM, therefore, the O-fCDs based sensing platform can satisfy the requirements of biomedical analysis such as iron metabolism monitoring and anemia diagnosis.

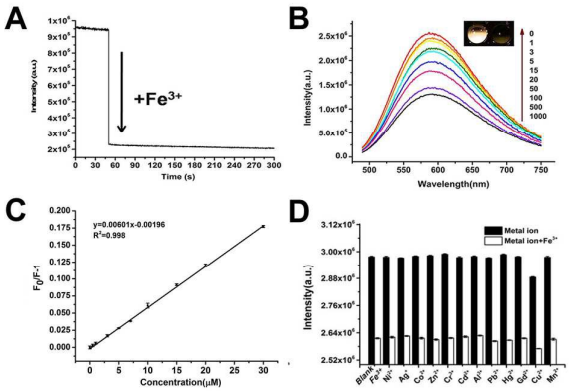

Figure 6. (A) PL intensity of the O-fCDs versus time in the presence of 50.0 μM Fe^{3+}. (B) PL emission spectra of the O-fCDs in the presence of various concentrations of Fe^{3+}. The insets are photographic images of O-fCDs in the absence and presence of 1.0 mM Fe^{3+}. (C) Stern-Volmer plot as a function of Fe^{3+} concentration. (D) The specificity of the O-fCDs nanoprobe (500 μg·mL^{-1}) to various metal ions in aqueous solution. The black bars represent the addition of interference metal ions (50.0 μM) in the absence of Fe^{3+}, and the white bars represent the addition of interference metal ions (50.0 μM) in the presence of 50.0 μM Fe^{3+}.

The response of O-fCDs towards other metal ions, including Ag^{+}, Cu^{2+}, Zn^{2+}, Co^{2+}, Hg^{2+}, Al^{3+}, Mn^{2+}, Pb^{2+}, Cd^{2+}, Cr^{3+}, Gd^{3+} and Ni^{2+}, were investigated in the absence and presence of Fe^{3+}, in order to evaluate the specificity of the present nanosensing platform. As shown in Figure 6D, no obvious PL changes were observed for any inspected metal ions, except that a small interference on the O-fCD-based nanosensing platform was detected for Cu^{2+}. Anyway, Fe^{3+} shows the most obvious quenching effect on the PL intensity of O-fCDs, as compared with other metal ions. The high sensitivity together with the high specificity which might be attributed to the strong affinity between Fe^{3+} and oxygen-containing groups on O-fCD surface

Table 2. Determination of Fe^{3+} in human serum samples using the O-fCDs based nanosensing platform and ICP-MS.

Sample	Spiked (μM)	Found by ICP-MS (μM)	Found by the present assay (μM)	Recovery ± SD (%, n=3)
Human serum 1	0	9.87	10.17 ± 0.06	103.04 ± 0.60
Human serum 2	14.61	23.96	24.55 ± 0.09	100.26 ± 0.38
Human serum 3	16.56	25.77	27.16 ± 0.28	102.76 ± 1.08

[12,46,47], enables the O-fCD a promising nanosensing platform for Fe^{3+} detection with high efficiency.

Recently, tremendous attentions have been paid on developing new probes for Fe^{3+} detection in biomedical samples with higher efficiency, because as an indispensable metal in life forms, deficiency or excess accumulation of Fe^{3+} would induce serious health problems[49-56]. Compared to the other reported Fe^{3+} sensing platform, the present O-fCDs based nanosensing platform showed a better performance, such as wider detection range, rapider response, and especially longer wavelength excitation which favors the biomedical detection (Table S2), emphasizing its potential applications in bioanalysis and biomedical detection.

To test the practicality of the O-fCDs based nanosensing platform, we extended it to determine the concentration of Fe^{3+} in human serum. As an internationally recognized standard method, inductively coupled plasma mass spectrometry (ICP-MS) experiments were performed to determine the Fe^{3+} content in the same human serum samples. The PL intensity of O-fCDs decreased when the human serum samples were spiked with Fe^{3+} standard solutions. The recoveries of Fe^{3+} in all samples were in the range of 100 - 103% (Table 2), and there was no systematic difference between the present method and ICP-MS as suggested by a paired Student's t-test. These results illustrate the feasibility and capabilities of the O-fCDs based nanosensing platform for the determination of Fe^{3+} in complicated biological environment.

Conclusions

In summary, a facile hydrothermal approach is illustrated to adjust PL peaks of fCDs from blue, green to orange by tuning the passivating reagents in a step-by-step manner during the synthesis. Surface passivation significantly alters the surface status, resulting in fCDs with either stronger surface oxidation or N element doping that ultimately determine their PL properties. Further experiments demonstrate the feasibility and capabilities of the O-fCDs based nanosensing platform for the determination of Fe^{3+} with high sensitivity and specificity in complicated biological environment, providing an opportunity for its practical applications in clinical and biological fields.

Acknowledgements

The financial support from the Pearl River S&T Nova Program of Guangzhou (2013J2200053), Guangdong special support program for high-level personnel (2014TQ01R417), and Guangdong Innovative Research Team Program (2009010057) is gratefully acknowledged.

Notes and references

1 C. Q. Ding, A. W. Zhu and Y. Tian, *Accounts Chem. Res.*, 2014, **47**, 20.
2 H. Li, Z. Kang, Y. Liu and S. T. Lee, *J. Mater. Chem.*, 2012, **22**, 24230.
3 H. J. Sun, L. Wu, W. L. Wei and X. G. Qu, *Mater. Today*, 2013, **16**, 433.
4 S. N. Baker and G. A. Baker, *Angew. Chem. Int. Ed.*, 2010, **49**, 6726.
5 P. G. Luo, S. Sahu, S. T. Yang, S. K. Sonkar, J. P. Wang, H. F. Wang, G. E. LeCroy, L. Cao and Y. P. Sun, *J. Mater. Chem. B*, 2013, **1**, 2116.
6 L. P. Lin, M. C. Rong, F. Luo, D. M. Chen, Y. R. Wang and X. Chen, *Trac-Trends Anal. Chem.*, 2014, **54**, 83.
7 Y. F. Wang and A. G. Hu, *J. Mater. Chem. C*, 2014, **2**, 6921.
8 K. Hola, Y. Zhang, Y. Wang, E. P. Giannelis, R. Zboril and A. L. Rogach, *Nano Today*, 2014, **9**, 590.
9 Y. F. Wang and A. G. Hu, *J. Mater. Chem. C*, 2014, **2**, 6921.
10 S. Y. Lim, W. Shen and Z. Q. Gao, *Chem. Soc. Rev.*, 2015, **44**, 362.
11 H. Y. Liu, Z. M. He, L. P. Jiang and J. J. Zhu, *ACS Appl. Mater. Inter.*, 2015, **7**, 4913.
12 S. W. Yang, J. Sun, X. B. Li, W. Zhou, Z. Y. Wang, P. He, G. Q. Ding, X. M. Xie, Z. H. Kang and M. H. Jiang, *J. Mater. Chem. A*, 2014, **2**, 8660.
13 S. Do, W. Kwon and S. W. Rhee., *J. Mater. Chem. C*, 2014, **2**, 4221.
14 D. Sun, R. Ban, P. H. Zhang, G. H. Wu, J. R. Zhang and J. J. Zhu, *Carbon*, 2013, **64**, 424.
15 J. Zhou, Y. Yang and C. Y. Zhang, *Chem. Commun.*, 2013, **49**, 8605.
16 Y. Q. Zhang, D. K. Ma, Y. Zhuang, X. Zhang, W. Chen, L. L. Hong, Q. X. Yan, K. Yu and S. M. Huang, *J. Mater. Chem.*, 2012, **22**, 16714.
17 Z. C. Yang, M. Wang, A. M. Yong, S. Y. Wong, X. H. Zhang, H. Tan, A. Y. Chang, X. Li and J. Wang, *Chem. Commun.*, 2011, **47**, 11615.
18 C. Hu, C. Yu, M. Y. Li, X. N. Wang, J. Y. Yang and Z. B. Zhao, *Small*, 2014, **10**, 4926.
19 S. L. Hu, A. Trinchi, P. Atkin and I. Cole, *Angew. Chem. Int. Ed.*, 2015, **54**, 2970.
20 L. Bao, C. Liu, Z. L. Zhang and D. W. Pang, *Adv. Mater.*, 2015, **27**, 1663.
21 B. P. Qi, H. Hu, L. Bao, Z. L. Zhang, B. Tang, Y. Peng, B. S. Wang and D. W. Pang, *Nanoscale*, 2015, **7**, 5969.
22 K. Jiang, S. Sun, L. Zhang, Y. Lu, A. G. Wu, C. Z. Cai and H. W. Lin, *Angew. Chem. Int. Ed.*, 2015, **54**, 5360.
23 S. J. Zhu, J. H. Zhang, S. J. Tang, C. Y. Qiao, L. Wang , H. Y. Wang, X. Liu, B. Li, Y. F. Li, W. L. Yu, X. F. Wang, H. C. Sun and B. Yang, *Adv. Funct. Mater.*, 2012, **22**, 4732.
24 L. Bao, Z. L. Zhang, Z. Q. Tian, L. Zhang, C. Liu, Y. Lin, B. P. Qi and D. W. Pang, *Adv. Mater.*, 2015, **23**, 5801.
25 X. H. Li and Z. W. Zhao, *RSC Adv.*, 2014, **4**, 57615.

26 S. K. Bhunia, A. Saha, A. R. Maity, S. C. Ray and N. R. Jana, *Sci. Rep.*, 2013, **3**, 1473.
27 H. Tetsuka, R. Asahi, A. Nagoya, K. Okamoto, I. Tajima, R. Ohta and A. Okamoto, *Adv. Mater.*, 2012, **24**, 5333.
28 Y. Q. Dong, R. X. Wang, H. Li, J. W. Shao, Y. W. Chi, X. M. Lin and G. N. Chen, *Carbon*, 2012, **50**, 2810.
29 Z. C. Yang, M. Wang, A. M. Yong, S. Y. Wong, X. H. Zhang, H. Tan, A. Y. Chang, X. Li and Y. Wang, *Chem. Commun.*, 2011, **47**, 11615.
30 S. H. Jin, D. H. Kim, G. H. Jun, S. H. Hong and S. Jeon, *ACS Nano*, 2013, **7**, 1239.
31 S. Zhu, Q. Meng, L. Wang, J. Zhang, Y. Song, H. Jin, K. Zhang, H. Sun, H. Wang and B. Yang, *Angew. Chem. Int. Ed.*, 2013, **52**, 3953.
32 Y. P. Shi, Y. Pan, H. Zhang, Z. M. Zhang, M. J. Li, C. Q. Yi and M. S. Yang, *Biosens. Bioelectron.*, 2014, **56**, 39.
33 Z. M. Zhang, Y. P. Shi, Y. Pan, X. Cheng, L. L. Zhang, J. Y. Chen, M. Li and C. Q. Yi, *J. Mater. Chem. B*, 2014, **2**, 5020.
34 V. Strauss, J. T. Margraf, C. Dolle, B. Butz, T. J. Nacken, J. Walter, W. Bauer, W. Peukert, E. Spiecker, T. Clark and D. M. Guldi, *J. Am. Chem. Soc.*, 2014, **136**, 17308.
35 R. J. Fan, Q. Sun, L. Zhang, Y. Zhang and A. H. Lu, *Carbon*, 2014, **71**, 87.
36 Y. P. Shi, Y. Pan, J. Zhong, J. Yang, J. H. Zheng, J. L. Cheng, R. Song and C. Q. Yi, *Carbon*, 2015, **93**, 742.
37 A. S. Karakoti, S. Das, S. Thevuthasan and S. Seal, *Angew. Chem. Int. Ed.*, 2011, **50**, 1980.
38 R. L. Liu, D. Q. Wu, S. H. Liu, K. Koynov, W. Knoll and Q. Li, *Angew. Chem. Int. Ed.*, 2009, **48**, 4598.
39 Y. P. Sun, B. Zhou, Y. Lin, W. Wang, K. A. S. Fernando, P. Pathak, M. J. Meziani, B. A. Harruff, X. Wang, H. F. Wang, P. J. G. Luo, H. Yang, M. E. Kose, B. L. Chen, L. M. Veca and S. Y. Xie, *J. Am. Chem. Soc.*, 2006, **128**, 7756.
40 X. Wang, L. Cao, S. T. Yang, F. S. Lu, M. J. Meziani, L. L. Tian and K. W. Sun, *Angew. Chem. Int. Ed.*, 2010, **49**, 5310.
41 L. Cao, X. Wang, M. J. Meziani, F. Lu, H. Wang, P. G. Luo, Y. Lin, B. A. Harruff, L. M. Veca, D. Murray, S. Y. Xie and Y. P. Sun, *J. Am. Chem. Soc.*, 2007, **129**, 11318.
42 G. E. LeCroy, S. K. Sonkar, F. Yang, L. M. Veca, P. Wang, K. N. Tackett, J. J. Yu, E. Vasile, H. J. Qian, Y. M. Liu, P. J. Luo and Y. P. Sun, *ACS Nano*, 2014, **8**, 4522.
43 S. Zhu, S. Tang, J. Zhang and B. Yang, *Chem. Commun.*, 2012, **48**, 4527.
44 D. Qu, M. Zheng, L. G. Zhang, H. F. Zhao, Z. G. Xie, X. B. Jing, R. E. Haddad, H. Y. Fan and Z. C. Sun, *Sci. Rep.*, 2014, **4**, 5294.
45 C. F. Wang, D. Sun, K. L. Zhuo, H. C. Zhang and J. J. Wang, *RSC Adv.*, 2014, **4**, 54060.
46 Y. Liu, N. Xiao, N. Q. Gong, H. Wang, X. Shi, W. Gu and L. Ye, *Carbon*, 2014, **68**, 258.
47 Y. L. Zhang, L. Wang, H. C. Zhang, Y. Liu, H. Y. Wang, Z. H. Kang and S. T. Lee, *RSC Adv.*, 2013, **3**, 3733.
48 Y. B. Song, S. J. Zhu, S. Y. Xiang, X. H. Zhao, J. H. Zhang, H. Zhang, Y. Fu and B. Yang, *Nanoscale*, 2014, **6**, 4676.
49 Y. Y. Du, M. Chen, Y. X. Zhang, F. Luo, C. Y. He, M. J. Li and X. Chen, *Talanta*, 2013, **106**, 261.
50 R. R. Crichton, D. T. Dexter and R. J. Ward, *Monatsh. Chem.*, 2011, **142**, 341.
51 R. H. Crabtree, *Science*, 1994, **266**, 1591.
52 D. Carolan, H. Doyle, *Nanoscale*, 2015, **7**, 5488.
53 L. He, J. N. Li, J. H. Xin, *Biosens. Bioelectron.*, 2015, **70**, 69.
54 A. Ananthanarayanan, X. W. Wang, P. Routh, B. Sana, S. Lim, D. H. Kim, K. H. Lim, J. Li, P. Chen, *Adv. Funct. Mater.*, 2014, **24**, 3021.
55 S. W. Zhang, J. X. Li, M. Y. Zeng, J. Z. Xu, X. K. Wang, W. P.Hu, *Nanoscale*, 2014, **6**, 4157.
56 S. N. Qu, H. Chen, X. M. Zheng, J. S. Cao, X. Y. Liu, *Nanoscale*, 2013, **5**, 5514.